Technical Physics, Vol. 46, No. 12, 2001, pp. 1537–1544. Translated from Zhurnal Tekhnicheskoĭ Fiziki, Vol. 71, No. 12, 2001, pp. 50–57.

SOLID-STATE ELECTRONICS

Film Carriers for Super-High-Density Magnetic Storage

G. I. Frolov

Kirenskiĭ Institute of Physics, Siberian Division, Russian Academy of Sciences, Akademgorodok, Krasnoyarsk, 660036 Russia

Received February 27, 2001

Abstract—The problem of increasing the recording density in magnetic storage devices is considered. It is shown that nanograined magnetic film media are candidate materials for magnetic data carriers. For these materials to completely meet the requirements for super-high-density magnetic carriers, appropriate structure ordering must be set in the films. To this end, it is suggested to take advantage of the high adsorbability of 3*d* metal nanoparticles on high-molecular compounds. To produce the carriers based on these materials with a recording density of as high as 10^{10} bit/cm^2, nanoparticles of size ≤ 5 nm should be embedded in a polymer matrix. To do this, it is necessary to combine chemical and physical methods for nanocomposite production. © *2001 MAIK "Nauka/Interperiodica".*

INTRODUCTION

It seems quite realistic that science and technology of the 21st century will deal with nanometer- or even angström-size (quantum) objects, since many of the conventional microelectronic technologies are approaching or have already reached the fundamental (classical) limits of miniaturization. This stimulates the search of alternative lines of attack. Since the properties of a solid depend on its chemical composition, atomic structure, and dimensionality, the transition from a 3D (massive) body to an object whose dimensions in one, two, or three directions are as small as several interatomic spacings leads to a change in the physicochemical properties of the material. The specific properties of materials structured on the nanolevel (hereafter called nanostructured materials) provide the basis for the development of new-generation electron devices as microelectronics is now steadily passing from the micro- to the nanometer scale. An example is the breakthrough in the recording density of magnetic storage devices.

THE TRANSITION FROM MAGNETOOPTIC RECORDING TO LONGITUDINAL MAGNETIC RECORDING

In 1983, the US Commission on Magnetic Materials was established with the aim to judge the worldwide and national levels of research in the field of magnetism and outline directions of further development. The brief report of the Commission was issued in 1985 [1]. It was stated, in particular, that fundamental research on the physics of magnetic phenomenon is of great importance, since magnetic materials are "perfect systems for studying and verifying the basic concepts of the physics of solids." On the other hand, it was reported that the market of devices based on magnetic materials progressively expands. Among new promising applications of magnetic materials, emphasis was placed on external magnetooptic computer memories.

This direction is closely related with further advances in computer technology, whose potentialities depend on the performance of data writing, storage, and processing devices. At that time, optical technology was considered as a very promising way of increasing the RAM capacity. As alternative materials (carriers for regenerative magnetooptic storage devices), film alloys of rare-earth and transition metals were brought to the fore. The parameters of these films met the requirements of RAM designers completely [2, 3]. In these devices, data writing and reading are carried out with a laser beam. The recording density is restricted by the diffraction limit of optical radiations used and amounts to $\approx 10^8$ bit/cm^2 [4]. The predictions of RAM designers were to a great extent realized: early in the 1990s, magnetooptic memory devices filled their niche in the computer market [5].

Next item on the agenda was to devise still denser memories. In 1990, the idea of developing magnetic memory with a record density of $\approx 1.5 \times 10^8$ bit/cm^2 based on longitudinal recording was put forward [6]. In 1992, the technology of a magnetic memory with a record density of $\approx 1.5 \times 10^9$ bit/cm^2 was elaborated [7]. The new high technologies required novel materials whose properties depend on appropriately arranged structural nanoblocks. Let us consider the requirements for a magnetic carrier of recording density 1.5×10^9 bit/cm^2.

As is known, magnetically ordered materials consist of uniformly magnetized regions (domains) and transition regions (domain walls), where the magnetization varied from point to point. For a magnetic medium to be utilized for recording to the maximal extent, domain walls should be as thin as possible. The wall width W is

1063-7842/01/4612-1537$21.00

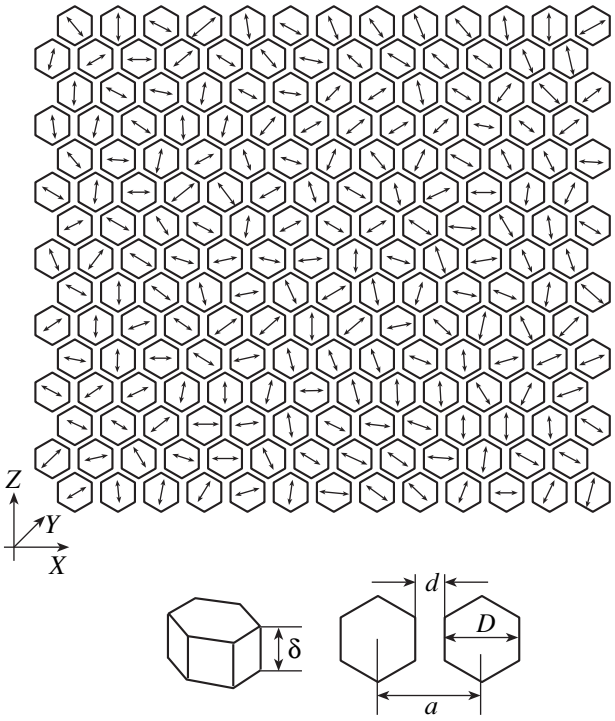

Fig. 1. Distribution of hexagonal grains in the *ZX* plane. The arrows indicate the directions of the easy axes of uniaxial anisotropy.

defined as $W = (A/K)^{1/2}$, where A is the exchange parameter and K is the anisotropy constant. The simplest way to make the wall thinner is to decrease A. This is easy to do in nanograined film materials where magnetic particles are separated from each other by a nonmagnetic spacer. Here, the particle size D is of great importance, since it specifies the signal-to-noise (S/N) ratio upon reading data. The value of D is calculated by the formula [8]

$$S/N = 10\log S/D^2,$$

where S is the area per bit. For a record density of 1.5×10^9 bit/cm^2 and S/N = 30–40 dB, D = 10–15 nm.

Now let us determine the basic magnetic parameters (coercive force H_c, remanent magnetization M_r, and the shape of hysteresis loop) of the nanograined films with the particles of the nanometer size. Since in longitudinal magnetic media the magnetization vector lies in the carrier plane, a large demagnetizing field arises. The value of H_c should therefore be selected as a trade-off: on the one hand, it must exceed this demagnetizing field; on the other hand, the capabilities of the read head must be taken into account. For the given recording density, $H_c \approx 3000$ Oe. The value of M_r is determined by the formula [9]

$$a = [M_r\delta(h + \delta/2)/\pi H_c]^{1/2},$$

where a is the width of the transition region between bits, h is the head–carrier spacing, and δ is the width of the magnetic layer of the carrier.

For a = 13 nm, h = 20 nm, δ = 10 nm, M_r = 500 G. The carrier also must have a rectangular hysteresis loop with a high ratio M_r/M_s, where M_s is the saturation magnetization. The feasibility of producing nanograined films with such magnetic parameters has been discussed by Zhu and Bertram [10]. They estimated the effect of the magnetic film microstructure on magnetization reversal and the hysteresis shape. The thin-film medium is represented as the planar arrangement of hexagonal nanograins shown in Fig. 1. Here, δ is the width of the film, which coincides with that of the grains; D is the grain size in the ZX plane; d is the intergranular spacing; and $a = d + D$ is the lattice constant. Each of the grains is a single-domain particle where the magnetization is reversed by the coherent rotation of the magnetic moment. The calculation involves the coupled dynamic equations with the Landau–Lifshitz phenomenological damping parameter. In this model, the effect of the microstructure on magnetic hysteresis shows up through exchange and dipole–dipole interactions between the particles (Fig. 2). The inclusion of both interactions leads to an increase in the ration M_r/M_s and a decrease in H_c. If, however, the dipole–dipole interaction is significant, magnetization reversal causes a vortical domain structure to appear and the quadratic shape of the hysteresis loop becomes distorted. Strong exchange interaction between particles widens the transition region between the domains. Thus, it has been shown that the nanograined films with an appropriate microstructure can have parameters necessary for high-density memory applications.

Subsequently, such devices have been created. Figure 3 shows a typical structure of the carrier used in advanced memories with longitudinal writing [11]. The carrier consists of several layers of which we are interested primarily in the Cr underlayer and the Co magnetic layer. The grain size in the magnetic layer depends on the microstructure of the underlayer (Fig. 4). The underlayer is usually made of Cr and NiAl. As the magnetic layer, Co-based alloys with Cr, Ta, Pt, etc. admixtures are employed. With such carriers, a recording density of 3–4 $\times 10^3$ bit/cm^2 [12, 13] has been attained. Memories with a recording density of up to 1.5×10^6 bit/cm^2 are predicted to appear in the former half of the current decade [14]. Several years ago, the problem of creating memory devices with a recording density as high as $\geq 10^{10}$ bit/cm^2 has been posed [15, 16].

REQUIREMENTS FOR MAGNETIC CARRIERS WITH A RECORDING DENSITY OF $\geq 10^{10}$ bit/cm^2

As a carrier for super-high-density memories, quantum magnetic disks have been suggested [15]. In these

disks, bits are single-domain particles in the form of a column or a strip that are evenly spaced in a nonmagnetic matrix. The shape and the form of each of the bits are selected such that their magnetic moments have only two oppositely directed quantum states of the same amplitude. The idea of quantum magnetic disks is by far very promising but requires much investigation into writing and reading processes and the development of the reliable technology.

It therefore seems logical to consider the potentialities of nanograined magnetic films as a medium for super-high-density ($\geq 10^{10}$ bit/cm^2) devices. Consider the requirements for the parameters of the films. Since the bit size decreases as the recording density grows, the demagnetizing field in longitudinal-writing media naturally increases; hence, H_c must be no less than 5000 Oe [16]. To keep the ratio S/N at a high level during data reading, the size of the magnetic particles must not exceed 5 nm. This raises the question as to whether there is a possibility of obtaining the desired parameters in the films considered.

It is known that the properties of the nanograined films depend on the properties of the nanoparticles and on the interactions between them. Let us see how the magnetic properties (M_s, H_c, and the Curie temperature T_C) vary as the particle size decreases. The variation of M_s in nanoparticles was discussed as early as in the 1960s [17]. By comparing the exchange energy, which is the energy of magnetic ordering, with the energy of zero-point oscillation, it has been found that the ferromagnetic properties of 3*d* metal particles of size ≤1 nm disappear at any temperature. Later, the magnetization of free 3*d* metal clusters containing from 10 to 300 atoms was measured. The < 1-nm clusters were found to be magnetized at temperatures between 100 and 200 K [18], and the magnetization may even exceed M_s of the bulk material [19]. This effect is related to the increased number of localized 3*d* electrons in the nanoparticles [20].

In the 1980s, works where the effect of the particle size on the Curie temperature was considered appeared. Although T_c of the nanoparticles is lower than in the bulk material, it was estimated at 500–600 K even for particles of size 1.0–1.5 nm [21].

As the magnetic particle size decreases, the coercive force becomes more difficult to measure. A typical H_c vs. D dependence is shown in Fig. 5 [22]. As the particle size diminishes from 40 to 20 nm, H_c grows, because the particles pass into the single-domain state. On further decreasing D, the coercive force sharply drops. This is associated with growing thermal fluctuations in the directions of the magnetic moment M of the particle. The magnetic moment M tends to align with the direction of easy magnetization, which is defined by the magnetic anisotropy of the particle. For M to deviate from this direction, it is necessary to overcome the energy barrier KV (V is the particle volume). The magnetic moment direction starts to noticeably fluctuate when the mean thermal energy k_BT (k_B is the Boltzmann constant) becomes comparable to the energy of anisotropy. At $k_BT_b = KV$ (T_b is the blocking temperature), a magnetic particle ensemble subjected to an external magnetic field and temperature behaves as a paramagnetic molecular gas with the only exception that the directions of the magnetic moment of the particles, not molecules, vary in the particle ensemble. This phenomenon has been called superparamagnetism [17]. In this case, the temperature dependence of the coercive

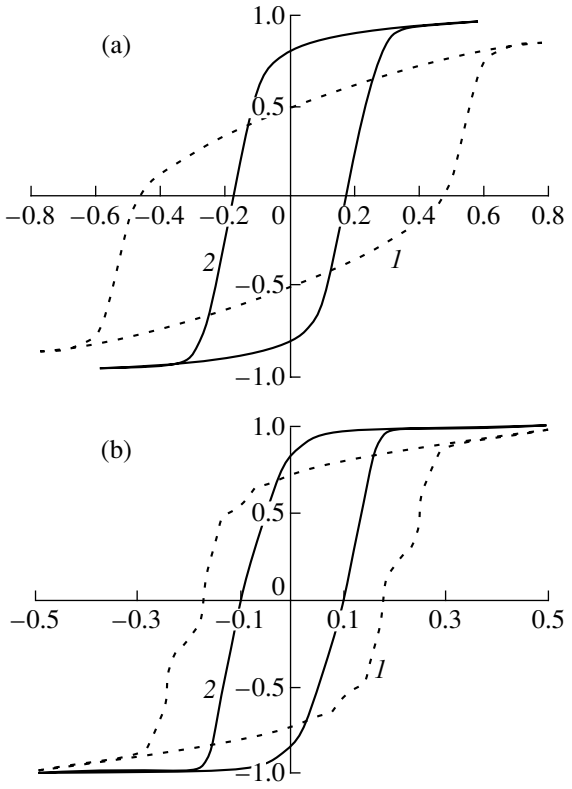

Fig. 2. Hysteresis loop for volume-disordered anisotropy axes. (a) Exchange interaction between the grains is absent, $\delta/a = 0.5$, dipole–dipole interaction $M/H_k = (1)$ 0 and (2) 0.4 (H_k is the anisotropy field); (b) $M/H_k = 0.4$, $\delta/a = 0.75$, exchange interaction is (1) 0 and (2) 0.15.

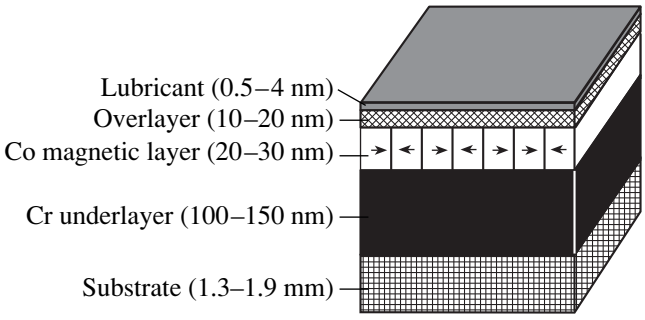

Fig. 3. Carrier for longitudinal writing.

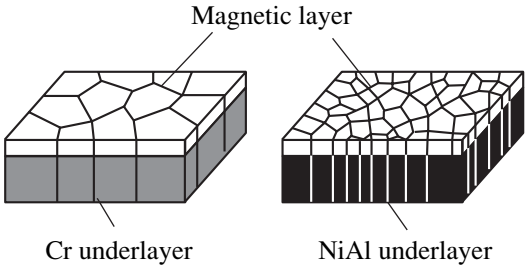

Fig. 4. Effect of the underlayer structure on the magnetic layer structure.

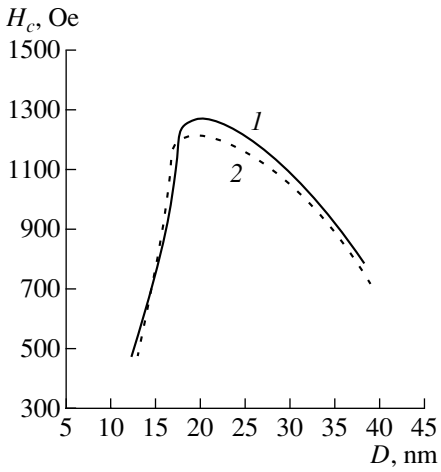

Fig. 5. Coercive force vs. Fe grain size. The particles were deposited in the (*1*) O_2 and (*2*) N_2 atmosphere.

force is given by [11]

$$H_c = H_{c0}[1 - (T/T_b)^{1/2}].$$

As follows from this expression, the coercive force can be increased by increasing the temperature of transition to the superparamagnetic state. To do this, one must raise the magnetic anisotropy constant of the particles. This can be done in three ways: (1) by using materials with a high crystallographic anisotropy (Co–Sm, Co–Pt, and like alloys), (2) by varying the shape of the particles (from spherical to elongated [23]), and (3) by inducing the anisotropy in a particle ensemble via exchange and dipole–dipole interactions. While the first two approaches have already been applied in producing novel magnetic carriers, the last one has not yet been implemented. For example, the effect of exchange and dipole–dipole interactions on the hysteresis loop has been considered only for the case of a one-layer nanostructured film [10]. At the same time, the interaction between magnetic particles has received much attention. Let us address ourselves to the results obtained in [24].

In [24], the conditions for ferromagnetic ordering in a set of single-domain particles interacting with each other are found in the mean field approximation. The set is comprised of spherical ferromagnetic particles of radius $D/2$ embedded in a solid nonmagnetic matrix. The distribution of the particles in the matrix is simulated under the assumption that their centers occupy (with a probability p) the sites of the tetragonal lattice having the periods d_1 (along the X and Y axes) and d_2 (along the Z axis, which is the tetrad axis). It is assumed that the interaction between the particles is magnetic dipole, the particles are uniaxial, their axes of easy magnetization are perpendicular to the XY plane, and the dynamics of the magnetic moment for any of the particles is described by the stochastic Landau–Lifshitz equation.

It has been established the ferromagnetic ordering in this system takes place at $d_2/d_1 < 1$. As the radius of the particles grows, the superparamagnetic–ferromagnetic phase transition temperature T_l rapidly approaches the Curie temperature of the bulk material. For example, for a set of single-domain Co particles ($p = 1$, $d_2/d_1 = 0.5$, and $d_2 = 3D/2$), the ratio T_b/T_C changes from 0.25 to 0.7 with $D/2$ varying from 2.5 to 3.5 nm.

The physical reason for the presence (at $d_2/d_1 < 1$) or absence ($d_2/d_1 \geq 1$) of ferromagnetic ordering in this system is the competition between magnetic dipole interactions between the particles. The particles surrounding some arbitrary chosen one can be subdivided into two groups according to their positions. Those of the first group produce a mean magnetic dipole field at the central particle chosen, this field being parallel to the magnetization vector, while the particles of the other group produce an antiparallel field. Ferromagnetic ordering occurs when the particles of the first group make a major contribution to the total dipole field, which takes place at $d_2/d_1 < 1$.

The result obtained indicates that a certain structure ordering in a set of interacting magnetic particle substantially raises the superparamagnetic–ferromagnetic phase transition temperature. With the beneficial effects due to the first and second approaches added, one may expect a significant rise in this temperature even for ≤5 nm particles.

From the aforesaid, it can be concluded that nanograined magnetic films with an ordered arrangement of the nanoparticles can meet the requirements for longitudinal recording carriers with a recording density above 10^{10} bit/cm^2.

FORMATION OF AN ORDERED STRUCTURE IN NANOGRAINED MAGNETIC FILMS

Ways for tackling the problem should be looked for in the new field of chemistry, so called supramolecular chemistry [25]. The subject of supramolecular chemistry is the synthesis and study of molecular ensembles (including clusters) with the self-organization properties. While conventional chemistry deals largely with reactions that break or produce valence bonds, supramolecular chemistry studies almost exclusively

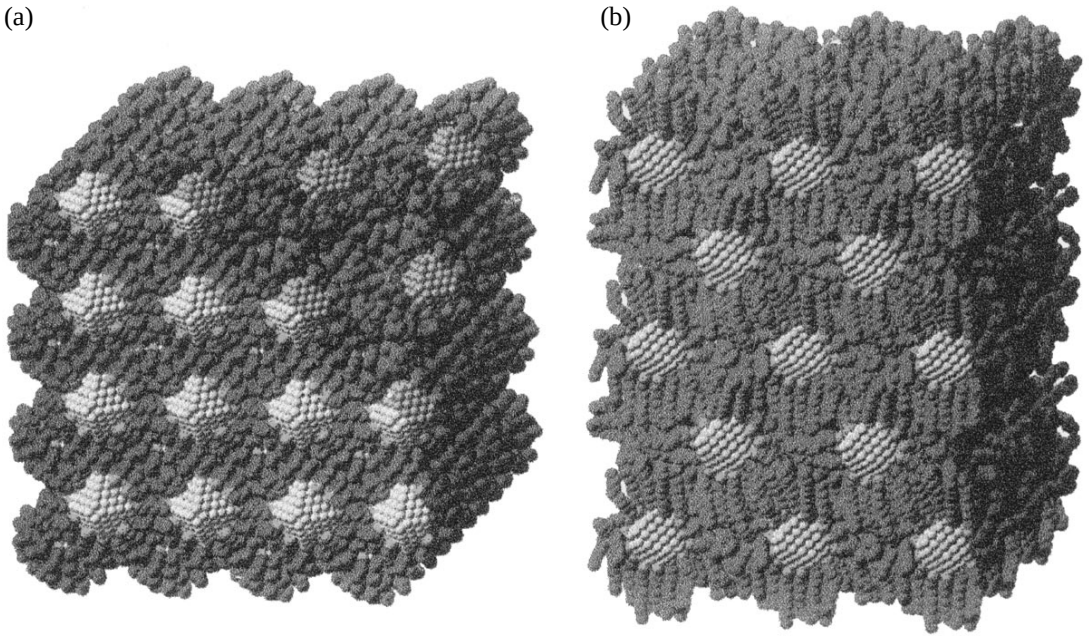

Fig. 6. Au nanoparticles are assembled into the (a) bcc and (b) *t*-fcc lattice.

nonvalent interactions, such as weak hydrogen bonds, electrostatic interaction, etc. The energy of these bonds are one to two orders of magnitude lower than the energy of valence ones; however, when combined, many such bonds may produce associates that are stable and at the same time readily change their structure.

Metal nanoparticles are highly reactive and have the developed surface. Accordingly, they are involved in a variety of spontaneous processes. To improve their stability is a basic challenge. For this purpose, various stabilizers are employed. One widely used approach is to stabilize metal nanoparticles with high-molecular compounds. The result is composites where ultradisperse particles or clusters are randomly distributed in a polymer matrix [26].

In recent years, the ensembles of passivated metal nanoparticles with the self-assembly properties have received much attention. Luedtke and Landman [27] studied the structure, dynamics, and thermal dynamics of ensembles of alkyl siloxane–passivated gold nanoparticles. The position and the concentration of the monolayers passivating the faces of the gold nanograins indicated that the monolayers are assembled like molecular packets of preferred orientation. On heating, this ordered state reversibly passes to the random intermolecular distribution. The equilibrium arrangement of adsorbed nanograins depends on the length of a molecular chain involved in passivation. If passivation is through a chain of $Au_{140}(C_4H_9S)_{62}$ molecules, the bcc superlattice forms at room temperature (Fig. 6a), which transforms into the fcc one on heating. At T = 300 K, the equilibrium superlattice of $Au_{140}(C_{12}H_{25}S)_{62}$ nanograins represents the tetragonally distorted fcc structure (*t*-fcc in Fig. 6b). The strength of the superlattices is due to the interaction between packet molecules. The superlattice parameters are $a \approx 2.9$ nm for the bcc and $a = b \approx 4.3$ nm, $c \approx 5.1$ nm for the *t*-fcc. Such ordered structures may be stable up to T = 800–900 K [28].

Subsequently, Yin and Wang [29] produced superlattices based on 3*d* metal nanograins. However, their technology concealed the danger of oxidizing 3*d* metal nanoparticles. To refine the resulting mixture, the metal particles were extracted by magnetic separation. Therefore, superlattices based on CoO nanoparticles were studied. The particles had the form of a tetrahedron (the edge length ≈4.4 nm) and form the fcc superlattice (with the parameter $a \approx 12$ nm). On heating to 600°C, the ordered structure breaks down, and a mixture of Co_2C and Co_3C nanograins instead of CoO results.

The materials described above were produced by the chemical method (the solution reduction of the metal compounds in the presence of stabilizers). This method is inappropriate for producing purely magnetic materials. Therefore, the need for physical methods (phase transitions of the first order in the absence of chemical reactions) to obtain nanograined magnetic films has emerged. Here, condensation methods have received the widest acceptance. Their essence is the assembly of the nanoparticles from individual metal atoms with the use of molecular or cluster beams. The atoms are then grouped together to produce a cluster that becomes a nucleus of the new phase once it has reached a certain size and exhibited the clear-cut physical interface.

At first glance, the cluster beam technology seems to be the most adequate solution to this problem. Mate-

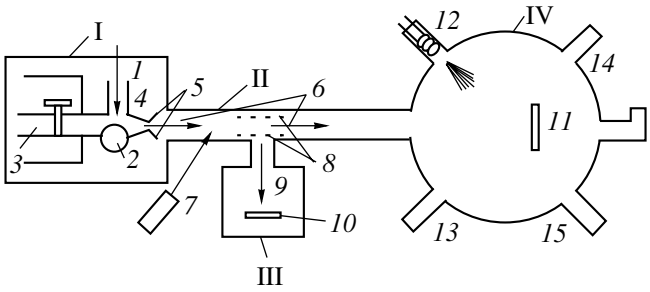

Fig. 7. Setup for evaporative deposition of the films from a neutral cluster beam. I, cluster generation chamber; II, cluster transport tube; III, chamber of cluster ion detector; IV, deposition chamber; *1*, pulsed laser; *2*, target; *3*, tube and valve for pulsed injection of helium; *4*, nozzle; *5*, skimmer; *6*, cluster flux; *7*, excimer laser; *8*, accelerating grids; *9*, cluster ion flux; *10*, detector; *11*, substrate; *12*, evaporator of matrix material; *13*, ion beam for cleaning the substrate; *14*, Auger spectrometer; and *15*, diffractometer.

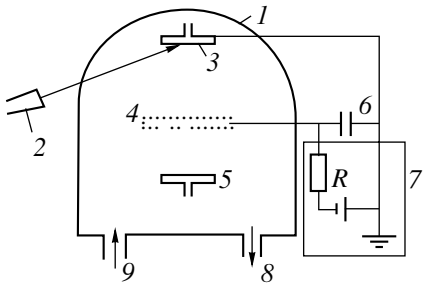

Fig. 8. Setup for evaporative deposition of the films from an atomic beam. *1*, Vacuum chamber; *2*, pulsed laser; *3*, target (cathode); *4*, circular electrode (anode); *5*, substrate; *6*, capacitor bank; *7*, bank charger; *8*, to pump; and *9*, working gas inlet.

rials thus obtained are thin films where clusters are embedded in an inert matrix. This technology has been applied by Perez *et al*. [30, 31]. They used a low-energy cluster beam to deposit nanograined films (including films of 3*d* metals). The associated setup is depicted in Fig. 7.

The generation of clusters is the most effective under nonequilibrium conditions, when the gas condenses into the bulk phase by cooling and the process ceases at the intermediate stage. Such conditions are the easiest to set when the gas or vapor freely flows out of a nozzle and expands to form a cluster beam. The target material is evaporated by a laser shot. Atoms evaporated are mixed with a buffer gas flow, and the subsequent expansion of the mixture into a vacuum through a nozzle leads to the formation of clusters. The mass of the clusters is measured with a time-of-flight mass spectrometer. Before the measurements, the clusters are irradiated by an excimer laser, ionized, accelerated, and directed to the measurement chamber. The neutral cluster flux strikes the substrate placed in the evaporation chamber.

The character of cluster–substrate interaction depends on the particle energy [32]. If the energy is low (<1 eV/atom), the cluster, when touching the surface, behaves as a liquid drop: initially, it adheres to the surface and produces a planar contact. Then, the surface (outer) atoms of the cluster spread over the surface due to diffusion, forming a thin film. When the cluster energy is high, the collision with the surface causes an appreciable shift of adjacent atoms, which results in the erosion of the surface material, followed by its evaporation. Therefore, low-energy cluster beams are used for depositing thin films. If several materials are sputtered simultaneously, a complex ensemble of solid clusters embedded in the matrix will condense. With this approach, nanograined films of various materials have been obtained in [30, 31, 33, 34].

However, the condensation of low-energy cluster beams to obtain nanograined films of 3*d* metals is a very complicated technology. Moreover, it does not have any obvious advantages over other simpler processes. The point is that the nanograin size in the resulting film depends largely on thermodynamic conditions under which the condensate forms rather than on the vapor flux type (atomic or cluster) [30, 31]. As a result, the nanograins have the same size when the films are deposited from atomic and cluster beams, all other things been equal.

To obtain nanograined magnetic films, we have suggested the method of pulsed plasma evaporation at a pressure of 10^{-6} torr [35–40]. Our setup is shown in Fig. 8. The method features a high condensation rate (~10^4 nm/s) at a pulse duration of ~10^{-4} s and at a cooling rate as high as ~10^8 K/s. This approach has turned out to be very efficient, since high vapor overcooling is the necessary condition for obtaining nanocrystalline systems [32]. In our method, a plasma is generated between the water-cooled anode and a 3*d* metal target being sputtered when a high-capacitance capacitor bank is discharged in the target vapor. An initial small amount of the vapor is produced by the laser evaporation of the target. The pulsed radiation of an LTI-207 solid-state laser partially evaporates the cathode material, producing the medium through which an electric current passes. The atoms evaporated are ionized in the discharge plasma. The resulting ions of the target atoms bombard the cathode, knocking out a new portion of the atoms. The evaporation process lasts for a time exceeding the pulse width by three or four orders of magnitude.

The novelty of our method is the proper choice of the ultimate dispersion of the crystalline structure when the number of originating nuclei is large and the radius of a critical nucleus coincides with that of coalescence. Films obtained with this method grow continuous, starting from thicknesses of 2 to 3 nm, and are comprised of nanograins of approximately the same size. This stems from the *in situ* measurements of the resistivity and the examination of the structures in tunnel

and high-resolution transmission electron microscopes. The parameters of the 3*d* metal films obtained with our method are similar to those of the films produced by the cluster beam technology: the grain sizes are equal, the local anisotropy constant is large, and the exchange parameter is relatively low.

Note, however, that the nanograined films of 3*d* metals obtained by the condensation of cluster and atomic beams have a low coercive force obviously because of the superparamagnetic effect. To rise the temperature of this transition, the films must be appropriately ordered. The ordering may be accomplished by taking advantage of the high adsorbability of the nanoparticles on high-molecular compounds. For example, one may deposit the metal nanoparticles in an appropriate atmosphere or sputter the metal and the polymer in parallel.

In this case, the new phase forms through the phase transition, but the synthesis of the final product involves chemical reactions [26]. Thin composite films may be prepared under conditions when the polymerization of related compounds and the vacuum evaporation of metals proceed concurrently. For example, the metallic target is sputtered in the glow discharge plasma of a polymer or compounds that will be used as matrices are sputtered in metal vapors. There can be versions where the vapors of a metal and of an organic solvent are codeposited onto a cooled substrate and the resulting condensate is heated to a certain temperature. In most of these cases, the material grows disordered. It becomes clear that the synthesis of structurally homogeneous nanocomposites is impossible if the matrix is not specially prepared. Therefore, a number of problems related to the vacuum condensation of the metallopolymeric phase and to the examination of its structure should be solved before the reliable technology of nanograined magnetic films with orderly arranged nanoparticles that combines physical and chemical methods is developed.

CONCLUSION

Thus, we showed that nanograined magnetic film media with nanoparticles of size ≤5 nm are competitive with magnetic quantum disks in the production of high-density magnetic memory devices.

The temperature of transition to the superparamagnetic state can be increased if certain structure ordering is established in these materials. To do this, one can take advantage of the high adsorbability of the nanoparticles on high-molecular compounds. In principle, the problem can be solved by chemical methods; however, dry (solution-free) processes for the formation of nanograined structurally ordered magnetic fields seem to be more appropriate for applications. Therefore, it is suggested to use technologies of vacuum deposition that combine physical and chemical methods.

Note, in conclusion, that ordered nanocomposites are not only of applied interest but also offer considerable scope for fundamental research.

REFERENCES

1. R. M. White, J. Appl. Phys. **57**, 2996 (1985).
2. L. V. Burkova and G. I. Frolov, Zarubezhn. Élektron., No. 9, 3 (1987).
3. G. I. Frolov, in *Magnetic Properties of Crystalline and Amorphous Media* (Nauka, Novosibirsk, 1989), pp. 218–234.
4. K. S. Aleksandrov, G. P. Berman, G. I. Frolov, and V. A. Seredkin, Proc. SPIE **1621**, 51 (1991).
5. M. D. Stoun, PC Magazine (USSR), No. 2, 11 (1991).
6. T. Yogi, C. Tsang, T. A. Nguyen, *et al.*, IEEE Trans. Magn. **26**, 2271 (1990).
7. E. S. Murdock, R. F. Simmons, and R. Davidson, IEEE Trans. Magn. **28**, 3078 (1992).
8. J. C. Mallinson, IEEE Trans. Magn. **5**, 182 (1969).
9. M. H. Kryder, W. Messner, and L. K. Garley, J. Appl. Phys. **79**, 4485 (1996).
10. J. G. Zhu and H. N. Bertram, J. Appl. Phys. **63**, 3248 (1988).
11. M. E. McHenry and D. E. Laughlin, Acta Mater. **48** (1), 223 (2000).
12. D. N. Lambeth, E. M. Velu, G. H. Bellesis, *et al.*, J. Appl. Phys. **79**, 4496 (1996).
13. H. Kisker, E. N. Abara, Y. Yamada, *et al.*, J. Appl. Phys. **81**, 3937 (1997).
14. I. Okamoto, I. Kaitsu, H. Akimoto, *et al.*, in *Digests of Intermag Conference, Korea, 1999*, AA-03.
15. S. Y. Chou, M. S. Wei, P. R. Kraus, and P. B. Fischer, J. Vac. Sci. Technol. B **12**, 3695 (1994).
16. E. S. Murdock, P. J. Ryan, J. F. Casto, *et al.*, in *Digests of Intermag Conference, Korea, 1999*, BA-02.
17. S. V. Vonsovskiĭ, *Magnetism* (Nauka, Moscow, 1971; Wiley, New York, 1974).
18. W. A. Heer, P. Milani, and A. Chatelain, Phys. Rev. Lett. **65**, 488 (1990).
19. J. P. Bucher, D. C. Douglass, and L. A. Bloomfield, Phys. Rev. Lett. **66**, 3052 (1991).
20. G. Gantefor and W. Eberhardt, Phys. Rev. Lett. **76**, 4975 (1996).
21. K. Kimura, Phys. Lett. A **158**, 85 (1991).
22. C.-M. Hsu, H.-M. Lin, and K.-R. Tsai, J. Appl. Phys. **76**, 4793 (1994).
23. H. Aharon, J. Appl. Phys. **41**, 5891 (1994).
24. S. I. Denisov, Fiz. Tverd. Tela (St. Petersburg) **41**, 1822 (1999) [Phys. Solid State **41**, 1672 (1999)].
25. A. F. Pozharskiĭ, Sorosov. Obraz. Zh., No. 9, 32 (1997).
26. A. D. Pomogaĭlo, A. S. Rozenberg, and I. E. Uflyand, *Nanoparticles of Metals in Polymers* (Khimiya, Moscow, 2000).
27. W. D. Luedtke and U. Landman, J. Phys. Chem. **100**, 13323 (1996).
28. S. A. Harfenist and Z. L. Wang, J. Phys. Chem. **103**, 4342 (1999).

29. J. S. Yin and Z. L. Wang, J. Phys. Chem. B **101**, 8979 (1997).
30. J. P. Perez, V. Dupuis, J. Tuaillon, *et al.*, J. Magn. Magn. Mater. **145**, 74 (1995).
31. A. Perez, P. Melinon, V. Dupuis, *et al.*, J. Phys. D **30**, 709 (1997).
32. B. M. Smirnov, Usp. Fiz. Nauk **167**, 1169 (1997) [Phys. Usp. **40**, 1117 (1997)].
33. J. Tuaillon, V. Dupuis, P. Melinon, *et al.*, Philos. Mag. A **76**, 493 (1997).
34. V. Dupuis, J. Tuaillon, B. Prevel, *et al.*, J. Magn. Magn. Mater. **165**, 42 (1997).
35. G. I. Frolov, V. S. Zhigalov, S. M. Zharkov, and I. R. Yarullin, Fiz. Tverd. Tela (St. Petersburg) **36**, 970 (1994) [Phys. Solid State **36**, 526 (1994)].
36. G. I. Frolov, O. A. Bayukov, V. S. Zhigalov, *et al.*, Pis'ma Zh. Éksp. Teor. Fiz. **61**, 61 (1995) [JETP Lett. **61**, 63 (1995)].
37. G. I. Frolov, V. S. Zhigalov, A. I. Pol'skiĭ, and V. G. Pozdnyakov, Fiz. Tverd. Tela (St. Petersburg) **38**, 1208 (1996) [Phys. Solid State **38**, 668 (1996)].
38. V. S. Zhigalov, G. I. Frolov, and L. I. Kveglis, Fiz. Tverd. Tela (St. Petersburg) **40**, 2074 (1998) [Phys. Solid State **40**, 1878 (1998)].
39. V. S. Zhigalov, G. I. Frolov, V. G. Myagkov, *et al.*, Zh. Tekh. Fiz. **68** (9), 136 (1998) [Tech. Phys. **43**, 1130 (1998)].
40. G. I. Frolov, V. S. Zhigalov, L. I. Kveglis, *et al.*, Fiz. Met. Metalloved. **88** (2), 85 (1999).

Translated by V. Isaakyan